Stochastic Optimization of Economic Dispatch With Wind and Photovoltaic Energy Using the Nested Sparse Grid-Based Stochastic Collocation Method

ZHILIN LU[1], MINGBO LIU[ID][1], (Member, IEEE), WENTIAN LU[ID][1], AND ZHUOMING DENG[ID][1,2]

[1]School of Electric Power Engineering, South China University of Technology, Guangzhou 510640, China
[2]Electric Power Research Institute, China Southern Power Grid, Guangzhou 510663, China

Corresponding author: Wentian Lu (hnlgtiantian@163.com)

ABSTRACT Due to the increasing uncertainty brought about by renewable energy, conventional deterministic dispatch approaches have not been very applicative. This paper investigates a nested sparse grid-based stochastic collocation method (NS-SCM) as a possible solution for stochastic economic dispatch (SED) problems. The SCM was used to simplify the scenario-based optimization model; specifically, a finite-order expansion using the generalized polynomial chaos (gPC) theory was applied to approximate random variables as a more facile approach compared to using complicated optimization models. Furthermore, a nested sparse grid-based approach was adopted to reduce the number of collocation points while still satisfying the nested property, thereby alleviating and effectively eliminating the need for computation. The proposed approach can be directly applied to the SED optimization problem. Lastly, simulations on the modified IEEE 39-bus system and a practical 1009-bus power system were provided to verify the accuracy, effectiveness, and practicality of the proposed algorithm.

INDEX TERMS Stochastic optimization, economic dispatch, generalized polynomial chaos, stochastic collocation method, Gauss-Hermite quadrature, sparse grid, nested property.

NOMENCLATURE
INDICES
ij Index of line, from bus i to bus j.
t Index of scheduling time interval.
g Index of conventional generator unit.
w Index of wind farm.
p Index of PV power generation.

SETS
G Index set of conventional generators.
T Index set of scheduling time intervals.
W Index set of wind farms.
P Index set of PV power generations.
Φ_G^i Index set of conventional generators at bus i.
Φ_W^i Index set of wind farms at bus i.

Φ_P^i Index set of PV power generations at bus i.
Γ Set of lines.
s Set of scenarios.
Ωi Set of buses connected to bus i.

PARAMETERS
ΔT Period between any two adjacent time intervals.
x_{ij} Reactance of line ij.
g_{ij} Conductance of line ij.
a_g Electricity generation cost of the gth conventional generator unit.
a_p Unit electricity generation cost of the pth PV power generation.
a_w Unit electricity generation cost of the wth wind farm.
r_{dg} Downward ramping rate limit of the gth conventional generator.

r_{ug}	Upward ramping rate limit of the gth conventional generator.
$P_{i,t}$	Active demand of load bus i at time interval t.
$P_{ij}^{\max}$	Maximum transmission power of line ij.
$P_{g,\min}$	Lower limit of the output of conventional generators.
$P_{g,\max}$	Upper limit of the output of conventional generators.
$P'_{w,t}$	Upper forecasted output of the wth wind farm at time interval t.
$P'_{p,t}$	Upper forecasted output of the pth PV power generation at time interval t.
l	Integral precision of MNI.
N_{ucp}	Number of univariate collocation points.
N_{uc}	Number of univariate scenarios.
N_{uss}	Number of univariate sampling scenarios.
N_{cp}	Number of collocation points.

VARIABLES

$\theta_{i,t}$	Voltage angle at bus i in interval t.
$P_{ij,t}$	Transmission power of line ij at time interval t.
$P_{loss,ij,t}$	The active power loss of line ij at time interval t.
$P_{w,t}$	Output of the wth wind farm at time interval t.
$P_{p,t}$	Output of the pth PV power generation at time interval t.
$P_{g,t}$	Output of the gth conventional generator unit at time interval t.
$P_{g,t}^{s}$	Output of the gth conventional unit at time interval t under the forecast scenario and the sampling scenarios.

ABBREVIATIONS

RES	Renewable energy sources
gPC	Generalized polynomial chaos
SED	Stochastic economic dispatch
SCM	Stochastic collocation method
NS-SCM	Nested sparse grid-based SCM
MNI	Multi-dimensional numerical integral

I. INTRODUCTION

The application of renewable energy sources (RES), especially wind farm and photovoltaic (PV) power generation stations, have increased in last five years [1]. Countries such as Denmark, Ireland, and Australia have aggressively installed RES systems and are operating with annual RES penetrations of more than 20% at the national level [2], [3]. Such a large-scale integration of high-penetration RES has raised significant challenges for the operation and dispatch of power systems because of the high intermittency and volatility of RES power. If its uncertainty is underestimated, the safety constraints of the system can be seriously destroyed, while overestimation can result in a sharp increase in the system operational cost [4]. Obviously, the existing dispatch methods cannot efficiently cope with the strong randomness and uncertainty of the RES. Therefore, it is significant to seek

approaches that are quite applicable for the stochastic economic dispatch (SED) problem with high-penetration RES.

A number of stochastic approaches have been utilized to solve the SED problem, including but not limited to chance-constrained optimization [5], [6], probabilistic power flow [8]–[12], robust optimization [13]–[17], and scenario-based method [19]–[25]. The chance-constrained optimization method obtains solutions within a certain probability; thus, it still risks violation of the constraints [7]. The robust optimization method employs a robust counterpart rather than a large number of scenarios. However, this approach may generate an obtained solution that may be too conservative and may oftentimes produce infeasibilities [18]. The scenario-based method is easier to implement as compared with chance-constrained and robust optimization, given that it decomposes the complex stochastic problem into simple subproblems that correspond to specific scenarios [19]–[21]. However, the scenario-based method can suffer from heavy computational burdens in the presence of high multi-dimensional random variables and large number of sampling scenarios [22]–[24]. Therefore, many scenario reduction techniques [20]–[23] have been proposed to overcome the computational complexity, although at the cost of losing the accuracy of the optimal solution.

Tang *et al.* presented an alternative idea for simplifying the scenario-based optimization model to achieve a better trade-off between the convergence speed and the problem size [26], where the uncertainty quantification (UQ) was used to create a surrogate model to solve the stochastic problem. In general, the effect of random variables can be resolved according to its probability distribution following the application of the Monte Carlo method [27]. However, this approach converges considerably slowly given the presence of the variable $1/\sqrt{N}$ [27] and often requires data from thousands of samples, thereby generating heavy computational burdens. The Stochastic Galerkin (SGM) and Stochastic Collocation methods (SCM) were recently proposed and utilized for the resolution of stochastic problems [28], [29]. Both SGM and SCM generate uncertainty analysis results based on the application of the generalized polynomial chaos (gPC) expansion theory on a polynomial of random variables. SCM can be performed without any additional alterations to the original model as compared to SGM, which has a more complicated calculation process. Therefore, a SCM-based approach can be considered as a "black box" in the uncertainty quantification analysis [30]. Tang *et al.* proposed the dimension-adaptive SCM to obtain high-dimensional probabilistic uncertainty quantification results with nonlinear dependence on the probabilistic power flow problem [26]. In comparison, Bai *et al.* proposed a dimension-reduced sparse grid strategy to improve the computational efficiency of the SCM [31]. Although both Tang *et al.* and Bai *et al.* presented SCM-derived algorithms that were designed to solve this type of problem without an optimization objective, their proposed methods cannot be directly applied to optimization problems such as the SED [26], [31]. Therefore, the present study attempted to

design an optimization algorithm to serve as a new extension to the SCM to solve the SED problem.

The contributions of this study are as follows:

- The SCM was applied to simplify the scenario-based optimization model, thereby improving the computational efficiency of the system with minimal loss of accuracy. The random variables were approximated through finite-order expansion by the application of the optimal gPC, thus eliminating the necessity of solving complicated optimization models with random variables.
- The sparse grid-based approach [40] was also employed to reduce the number of collocation points prior to calculating the gPC coefficients, which helped avoid dimensionality calculation issues. To further improve the computational efficiency, we proposed the nested sparse grid approach [40], by which the selected collocation point satisfied the nested property, to construct the collocation points.

The remainder of the paper is organized as follows: The SED model, which served as the bases, is formulated in Section II. Section III presents the SCM for random variables. Section IV discusses a solution for the multi-dimensional numerical integral (MNI) and applies the sparse grid approach to improve the computational efficiency. Section V puts forth the nested sparse grid-based stochastic collocation method (NS-SCM) for modeling. Section VI provides the numerical findings of the modified IEEE 39-bus and practical power systems. Finally, Section VII summarizes the observations to present the final conclusions.

II. MODEL OF THE STOCHASTIC ECONOMIC DISPATCH WITH RES

In general, the direct current (DC) power flow is applied to formulate the SED model without additional considerations for the transmission losses [31]–[35]. However, this approach does not guarantee the accuracy of the economic dispatch, especially in practical engineering applications. Therefore, the present study considered the transmission losses based on a modified direct current power flow model [36], [37]. Figure 1 shows the equivalent model of a transmission line with respect to its active power loss. The active power loss of line ij is presented as follows:

$$P_{loss,ij} = g_{ij}(\theta_i - \theta_j)^2, \qquad (1)$$
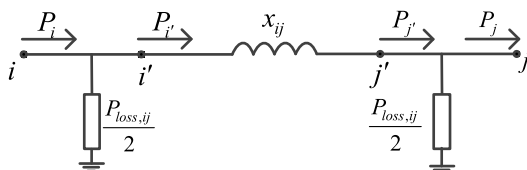

FIGURE 1. Equivalent model of the transmission line with respect to the active power loss.

The SED model, which aims to minimize the electricity costs generated by the conventional generators and RES, can be expressed as follows:

$$\min f = \sum_{t=1}^{T} \left(\sum_{g \in G} a_g P_{g,t} + \sum_{w \in W} a_w P_{w,t} + \sum_{p \in P} a_p P_{p,t} \right) \qquad (2)$$

$$\sum_{g \in \Phi_i^G} P_{g,t} + \sum_{w \in \Phi_i^W} P_{w,t} + \sum_{p \in \Phi_i^P} P_{p,t}$$
$$= P_{i,t} + P_{ij,t} + \sum_{j \in \Omega_i} \frac{P_{loss,ij,t}}{2}, \qquad (3)$$

$$\begin{cases} 0 \le P_{p,t} \le P'_{p,t} \\ 0 \le P_{w,t} \le P'_{w,t} \end{cases} \qquad (4)$$

$$P_{g\,\min} \le P_{g,t} \le P_{g\,\max} \qquad (5)$$

$$-r_{dg}\Delta T \le P_{g,t} - P_{g,t-1} \le r_{ug}\Delta T \qquad (6)$$

$$P_{ij,t} = (\theta_{i,t} - \theta_{j,t})/x_{ij} \qquad (7)$$

$$-P_{ij}^{\max} \le P_{ij,t} \le P_{ij}^{\max}, \quad \forall ij \in \Gamma \qquad (8)$$

In the above SED model, Equation (2) represents the objective of the model. Equation (3) represents the power balance constraint at bus i. Equation (4) describes the constraint of the output of the RES. Equations (5) and (6) describe the constraint of the output of conventional generators. Equations (7) and (8) represent the network transmission constraints.

III. SCM-BASED RANDOM VARIABLE APPROXIMATION

In general, RES outputs are not accurately predicted, as they randomly fluctuate around the predicted value. The Monte Carlo simulation and a scenario-based method (MCM-SBM) are generally applied to stabilize and resolve these RES uncertainties. However, when there are a high multi-dimensional random variable and a large number of sampling scenarios, MCM-SBM endures a heavy calculational burden. Therefore, the present study applied the SCM to simplify the scenario-based optimization model, thereby improving the computational efficiency with minimal loss of accuracy. The optimal gPC was applied to random variables to approximate a finite-order expansion, thus avoiding the need to resolve a complicated optimization model with random variables.

A. FORMULATION OF THE SED MODEL WITH RANDOM VARIABLES

The present study first defined the forecasted RES output errors as the input random parameters, the voltage angle of the buses and output of the RESs as the output random variables, and the conventional generator unit outputs as the deterministic variables. The SED model based on the stochastic problems is expressed as follows:

$$u\left(\overrightarrow{\xi}\right) = g\left(\boldsymbol{x}, \overrightarrow{\xi}\right) \qquad (9)$$

where $\boldsymbol{x}$ defines the vector of the deterministic variables, $\overrightarrow{\xi}$ is the deviation of the random parameter, and $u\left(\overrightarrow{\xi}\right)$

defines the vector of the output random variables, which can be approximated by applying the optimal gPC through finite-order expansion.

B. SCM THEORY
The present study first discussed one-dimensional normal random variables. According to the SCM theory, we can utilize the appropriate gPC to approximate the random variables corresponding to their distributions; hence, both the voltage angle of the buses and RES outputs were approximated by Hermite polynomial chaos expansion [38]. The process of solving Equation (9) by using SCM can be divided into three steps as follows:

Step 1: Choose an appropriate set of collocation points (sampling points) $\left\{ \overrightarrow{\xi_k} \right\}_{k=1}^{M}$ in the random parameter space.

Here, M defines the number of collocation points. The collocation points are the zero points of the M-order gPC as defined in the SCM theory, where $\overrightarrow{\xi}$ defines the normal random parameter and $u\left(\overrightarrow{\xi} \right)$ can be approximated by Hermite polynomial chaos expansion [38].

Step 2: Calculate a sequence of deterministic subproblems that correspond to a specific collocation point $\left\{ \overrightarrow{\xi_k} \right\}_{k=1}^{M}$, as presented in (9).

$$u\left(\overrightarrow{\xi_k} \right) = g\left(\boldsymbol{x}, \overrightarrow{\xi_k} \right), \quad i = 1, \ldots, M \qquad (10)$$

Equation (10) transformed the original stochastic equation (9) into M deterministic equations, which correspond to the collocation point $\left\{ \overrightarrow{\xi_k} \right\}_{k=1}^{M}$, thereby allowing the calculation of the deterministic solution $u\left(\overrightarrow{\xi_k} \right)$ for each subproblem.

Step 3: Use the gPC series expansion to approximate the random variables:

$$u\left(\overrightarrow{\xi} \right) = \sum_{q=0}^{\infty} \alpha_q \Phi_q\left(\overrightarrow{\xi} \right) \approx \sum_{q=0}^{N} \alpha_q \Phi_q\left(\overrightarrow{\xi} \right), \qquad (11)$$

where N defines the order of the expansion; α_q represents the unknown approximation coefficient, which can be computed by numerical integration; and $\Phi_q\left(\overrightarrow{\xi} \right)$ is a set of the one-dimensional gPC expressions that are used to approximate $u\left(\overrightarrow{\xi} \right)$. When the variables are multi-dimensional, they should be approximated by multi-dimensional polynomial, which is constructed by the one-dimensional ones [38].

The unknown α_q can be computed by numerical integration by obtaining the inner product for gPC in Equation (11) is due to the orthogonality of the gPC:

$$\alpha_q = \int_{\Gamma_\xi} u\left(\overrightarrow{\xi} \right) \Phi_r\left(\overrightarrow{\xi} \right) \rho\left(\overrightarrow{\xi} \right) d\overrightarrow{\xi}, \qquad (12)$$

where Γ_ξ and $\rho\left(\overrightarrow{\xi} \right)$ are the random parameter space and the joint probability density function of $\overrightarrow{\xi}$, respectively.

The right-hand side of Equation (12) is a continuous numerical integral, which allows its approximate computation by discrete numerical integration:

$$\alpha_q = \int_{\Gamma_\xi} u\left(\overrightarrow{\xi} \right) \Phi_r\left(\overrightarrow{\xi} \right) \rho\left(\overrightarrow{\xi} \right) d\overrightarrow{\xi}$$
$$\approx \sum_{k=1}^{M} u\left(\overrightarrow{\xi_k} \right) \Phi_r\left(\overrightarrow{\xi_k} \right) w_k, \qquad (13)$$

where w_k represents the quadrature weight corresponding to point $\left\{ \overrightarrow{\xi_k} \right\}_{k=1}^{M}$, and it is determined by the quadrature formula we chosen [39].

IV. SOLUTION OF MULTI-DIMENSIONAL NUMERICAL INTEGRAL
The typical economic dispatch analysis is related to some multivariate problems, such that the approximation coefficient α_q can be calculated using multi-dimensional numerical integral. Usually, the full grid-based stochastic collocation method (F-SCM) [40] is used to calculate α_q, but it may cause a combinatorial explosion. Therefore, the collocation point number can be reduced by applying the sparse grid approach prior to the gPC coefficients calculations, which helps eliminate dimensionality problems.

A. FULL GRID-BASED NUMERICAL INTEGRAL
In general, the F-SCM is applied to construct collocation points and compute the coefficient α_q of a d-dimensional random parameter $[\xi_1, \xi_2, \ldots \xi_d]$, specifically through its multi-dimensional numerical integral. The MNI can be constructed from one-dimensional ones [40]. Generally, a one-dimensional numerical integral $Q_1^{o_e}(f)$ of the e th variable with the o_eth level precision can be defined as follows:

$$\int g(\xi_e) \rho(\xi_e) d\xi_e \approx Q_1^{o_e}(f) \triangleq \sum_{u_e=1}^{n_1^{o_e}} g\left(\xi_{e,u_e}^{o_e} \right) w_{e,u_e}^{o_e}, \quad (14)$$

where $n_1^{o_e}$ is the total amount of collocation points (integration points) $\xi_{e,u_e}^{o_e}$ determined by the o_eth-level precision, and $W_{e,u_e}^{o_e}$ represents the quadrature weight corresponding to point $\xi_{e,u_e}^{o_e}$. Hence, the FSCM utilizes the full grid quadrature to calculate the multidimensional numerical integral in (12) by the tensor product as follows:

$$Q_d(f) \triangleq \int g\left(\overrightarrow{\xi} \right) \rho\left(\overrightarrow{\xi} \right) d\overrightarrow{\xi}$$
$$\approx \left(Q_1^{o_1} \otimes \cdots \otimes Q_1^{o_d} \right)(g)$$
$$= \sum_{u_1=1}^{n_1^{o_1}} \cdots \sum_{u_d=1}^{n_1^{o_d}} \left(w_{1,u_1}^{o_1} \times \cdots \times w_{d,u_d}^{o_d} \right) \cdot g\left(\xi_{1,u_1}^{o_1}, \cdots, \xi_{d,u_d}^{o_d} \right).$$
$$(15)$$

The total amount of integration points $\left\{ \xi_{1,u_1}^{o_1}, \cdots, \xi_{d,u_d}^{o_d} \right\}$ in (15) can be defined as follows:

$$N_{TPM} = n_1^{o_1} \times \cdots \times n_1^{o_d}. \qquad (16)$$

Suppose each integration point uses the same integral formula with the lth quadrature precision; then, N_{TPM} is equal to $\left(n_1^l\right)^d$, and will increase exponentially with respect to the dimensions due to dimensionality issues.

B. SPARSE GRID-BASED NUMERICAL INTEGRALS

To improve the computational efficiency by reduction of the number of integration points, the present study proposes the sparse grid-based stochastic collocation method (S-SCM) thereby addressing the combinatorial explosion brought by FSCM. The S-SCM in (14) employs sparse grid quadrature to calculate the multi-dimensional numerical integral in (12). The sparse grid quadrature of the d-dimensional variables with lth-level precision is defined as follows:

$$Q_d^l(f) \triangleq \sum_{l+1 \le |\overrightarrow{o}| \le l+d} (-1)^{l+d-|\overrightarrow{o}|} \binom{d-1}{l+d-|\overrightarrow{o}|} \times \left(Q_1^{o_1} \otimes \cdots \otimes Q_1^{o_d}\right)(g), \quad (17)$$

where $\overrightarrow{o}$ denotes the multi-index, and $|\overrightarrow{o}| = o_1 + o_2 + \cdots + o_d$. According to (17), $|\overrightarrow{o}|$ is present within the range of $l+1$ to $l+d$, such that one dimensional quadrature with a higher precision requires the other dimensions to use integral formulas with lower precisions. The set of integration points V_d^l with sparse grid quadrature in (15) can be expressed as follows:

$$V_d^l = \bigcup_{l+1 \le |\overrightarrow{o}| \le l+d} V_1^{o_1} \times \cdots V_1^{o_d}, \quad (18)$$

where the nodal set $V_1^{o_e}$ comprises the zeros of the Hermite polynomial of the eth variable with the o_eth-level, which can be expressed as follows:

$$\begin{aligned} V_1^1 &= \{0\} \\ V_1^2 &= \{-1, 1\} \\ V_1^3 &= \{-1.73, 0, 1.73\}, \\ &\quad \vdots \end{aligned} \quad (19)$$

where $n_1^{o_e}$ is defined as the number of one-dimensional integration points in $V_1^{o_e}$. Hence, n_d^l in V_d^l is defined as follows:

$$n_d^l = \sum_{l+1 \le |\overrightarrow{o}| \le l+d} n_1^{o_1} \cdots n_1^{o_d}. \quad (20)$$

In particular, when $l = 1, 2$, the number of integration points in V_1^d and V_2^d with sparse grid quadratures is defined as $n_d^1 = 2d+1$ and $n_d^2 = 2d^2+2d+1$, respectively. If $d \gg 1$, the total number of integration points is expressed as follows:

$$N_{TPM} = n_d^l \approx \frac{2^l}{l!} d^l. \quad (21)$$

Hence, N_{TPM} in the sparse grid does not increase exponentially with increasing dimensions as compared to what is generally observed in the full grid. As reported in (14) and (17),

the expression of the numerical integral on the basis of the sparse grid can be expressed as follows:

$$\begin{aligned} Q_d(g) \int g\left(\overrightarrow{\xi}\right) \rho\left(\overrightarrow{\xi}\right) d\overrightarrow{\xi} &\approx Q_d^l(g) \\ &= \sum_{l+1 \le |\overrightarrow{o}| \le l+d} \sum_{u_1=1}^{n_1^{o_1}} \cdots \sum_{u_d=1}^{n_1^{o_d}} g\left(\xi_{1,u_1}^{o_1}, \cdots, \xi_{d,u_d}^{o_d}\right) \\ &\quad \times w_{u_1, \cdots, u_d}^{o_1, \cdots, o_d}, \end{aligned} \quad (22)$$

where $w_{u_1, \ldots, u_d}^{o_1, \ldots, o_d}$ defines the quadrature weight corresponding to the integration point $\left(\xi_{1,u_1}^{o_1}, \cdots, \xi_{d,u_d}^{o_d}\right)$, which is expressed as:

$$w_{u_1, \cdots, u_d}^{o_1, \cdots, o_d} = (-1)^{l+d-|\overrightarrow{o}|} \binom{d-1}{l+d-|\overrightarrow{o}|} w_{e,u_1}^{o_1} \times \cdots \times w_{e,u_d}^{o_d}. \quad (23)$$

However, the conventional Gauss-Hermite quadrature nodal set determined by the zero points of the Hermite polynomial does not satisfy the nested property. That is, $V_1^1 \subseteq V_1^2 \subseteq \Psi V_1^3 \ldots$, such that collocation points with lower precisions cannot be reused in the quadrature nodal set with the higher precisions, thereby reducing the computational accuracy and efficiency.

V. NESTED SPARSE GRID-BASED STOCHASTIC COLLOCATION METHOD

In this section, the present study proposes a nested sparse grid-based stochastic collocation method (NS-SCM) with an extended Gauss-Hermite quadrature to enhance the calculational accuracy and efficiency of the S-SCM. The NS-SCM utilizes the one-dimensional extended Gauss-Hermite quadrature to construct the multi-dimensional nested sparse grid quadrature, thereby generating new collocation points that are based on existing collocation points with lower precision. The nested collocation points used in the NS-SCM not only maintain higher Gauss-Hermite quadrature calculational precision but also satisfy the nested property compared with applications in the S-SCM.

A. POLYNOMIAL PRECISION OF THE QUADRATURE

The present study first introduced the idea of polynomial space in Definition 1 to assess the accuracy of the Gauss-Hermite quadrature.

Definition 1: The univariate polynomial space $P(o_e)$ is defined as the space of all the polynomials in one variable, whose degrees do not exceed o_e.

According to Definition 1, the polynomial space $P(4)$ includes all linear combination of the polynomials whose degrees do not exceed 4 (*i.e.*, 1, ξ, ξ^2, ξ^3 and ξ^4). Hence, the polynomial precision of the Gauss-Hermite quadrature is defined as follows.

Definition 2: The integrand $g(\xi)$ in (13) is defined as any polynomial within the polynomial space $P(o_e)$. Therefore, if the integration can be strictly computed by the numerical

quadrature in (13), we can define the quadrature of $g(\xi)$ to be exact within the polynomial space $P(o_e)$.

In the Gaussian quadrature [39], a numerical integral with n integration points is exact within the polynomial space $P(2n-1)$. Therefore, the Gaussian quadrature of sets V_1^1, V_1^2, and V_3^1 in Section IV is accurate within the polynomial space $P(1)$, $P(3)$, and $P(5)$, respectively.

B. NUMERICAL INTEGRAL WITH ONE-DIMENSIONAL EXTENDED GAUSS-HERMITE QUADRATURE

Compared with the conventional Gauss-Hermite quadrature, a set of integration points with lower precision is contained in the set that presents higher precision in the extended Gauss-Hermite quadrature. Therefore, the nodal sets of collocation points do satisfy the nested property, which means that collocation points with lower precision can be reused in the quadrature nodal set with the higher precision.

For the Gauss-Hermite integral in (13), several families of univariate integration points with extended Gaussian-Hermite quadratures are proposed in [39]. To reduce the number of integration points, the present study chose the following nodal sequence with the slowest growth in points as follows:

$$\begin{cases} \tilde{V}_1^1 = \{0\} \\ \tilde{V}_1^2 = \{0, \pm 1.732\} \\ \tilde{V}_1^3 = \{0, \pm 1.732, \pm 4.18, \pm 0.74, \pm 2.86\} \\ \vdots \end{cases} \quad (24)$$

where $\tilde{V}_1^{o_e}$ denotes the nodal set of the extended Gauss-Hermite quadrature in one variable at the o_eth level. According to the definition in [38], the nodal sets, $\tilde{V}_1^1 \tilde{V}_1^2$, and $\tilde{V}_1^3$ with Gauss-Hermite quadrature in (24) are exact in the polynomial space $P(1)$, $P(5)$, and $P(15)$, respectively. In nodal set $\tilde{V}_1^2$, the uppermost quadrature accuracy of the three integration points is $P(5)$ following the addition of two integration points $\{\pm 1.732\}$ to the nodal set $\tilde{V}_1^1$. Similarly, the uppermost quadrature accuracy of those nine integration points in $\tilde{V}_1^3$ is $P(15)$. Therefore, the nodal sets of the zero points within the extended Gauss-Hermite quadrature in (24) do satisfy the nested property and can be expressed as $\tilde{V}_1^1 \subset \tilde{V}_1^2 \subset \tilde{V}_1^3 \subset \cdots$.

C. MULTI-DIMENSIONAL QUADRATURE WITH NESTED SPARSE GRIDS

The NS-SCM can be applied to compute the MNI in (14), of which the produced NS-SCM quadrature equation is similar to (17). However, the d-dimensional nested sparse grid quadrature with lth level precision in the NS-SCM generates a different nodal set as compared to that from in S-SCM [40], which is expressed as follows:

$$\tilde{V}_d^l = \bigcup_{|\vec{o}| \le l+d} \tilde{W}_1^{o_1} \times \cdots \tilde{W}_1^{o_1}, \quad (25)$$

where $\tilde{W}_1^{o_e}$ $(e = 1, \ldots, d)$ denotes the difference set between two adjacent nodal set $\tilde{V}_1^{o_e}$ and $\tilde{V}_1^{o_e-1}$ with extended

Gauss-Hermite quadrature, and it can be expressed as $\tilde{W}_1^{o_e} = \tilde{V}_1^{o_e} \backslash \tilde{V}_1^{o_e-1}$. Therefore, we obtain the following:

$$\begin{aligned} \tilde{W}_1^1 &= \tilde{V}_1^1 = \{0\} \\ \tilde{W}_1^2 &= \tilde{V}_1^2 \backslash \tilde{V}_1^1 = \{\pm 1.732\} \\ \tilde{W}_1^3 &= \tilde{V}_1^3 \backslash \tilde{V}_1^2 = \{\pm 4.18, \pm 0.74, \pm 2.86\} \\ &\vdots \end{aligned} \quad (26)$$

In (26), we define $\tilde{m}_1^{o_e}$ as the number of integration points in the nodal set $\tilde{W}_1^{o_e}$, such that the total amount of integration points used by NS-SCM is defined as:

$$\tilde{n}_d^l = \sum_{|\vec{o}| \le l+d} \tilde{m}_1^{o_1} \cdots \tilde{m}_1^{o_d}. \quad (27)$$

According to (27), increases in the quadrature degree increases from l to $l+1$ defines the $\tilde{W}_d^{l+1}$ as follows:

$$\tilde{W}_d^{l+1} = \bigcup_{|\vec{o}| = l+d} \tilde{W}_1^{o_1} \times \cdots \times \tilde{W}_1^{o_e}, \quad (28)$$

Hence, we obtain the following:

$$\tilde{V}_d^{l+1} = \tilde{V}_d^l \cup \tilde{W}_d^{l+1}. \quad (29)$$

From (29), the nodal set $\tilde{V}_d^{l+1}$ does appear to satisfy the nested property.

D. ALGORITHM FLOW

Figure 2 presents the algorithm based on the proposed NS-SCM to solve the SED model with RES as follows:

Step 1: Set the network topology based on the size of the systems, the number, and PDF of the input random variables, and the expansion order of the Hermite polynomial.

Step 2: Set the nodal set $\tilde{V}_1^{o_e}, o_e = 1, \cdots, l$ based on the order presented in (24).

Step 3: Compute the quadrature weight corresponding to the integration points with the extended Gauss-Hermite quadrature according to [39].

Step 4: Construct the nodal set $\tilde{V}_d^l$ with the MNI according to Equations (25) – (29).

Step 5: Calculate the quadrature weight $\tilde{w}_{u_1,\cdots,u_d}^{o_1,\cdots,o_d}$ with respect to the integration points $\left(\xi_{1,u_1}^{o_1}, \cdots, \xi_{d,u_d}^{o_d} \right) \in \tilde{V}_d^l$ and following the guidelines presented in [40].

Step 6: Utilize the solver to calculate the values of the output random variables with respect to each integration point, after which calculate α_q by applying Equation (22).

Step 7: Utilize the expansion of the Hermite polynomial to approximate the output random variables. Substitute the results into the original SED model to generate the surrogate SED model.

Step 8: Establish the constraints of the scenario transition to determine the adjustable output of the conventional generator units from the forecast scenario to the sampling scenarios, as defined in (30). Subsequently, utilize the MCM-SBM to simulate and approximate the surrogate SED model.

$$\begin{cases} -r_{dg}\Delta T \le P_{g,t}^0 - P_{g,(t-1)}^s \le r_{ug}\Delta T \\ g = 1, 2, \ldots, N_G; t = 1, 2, \ldots, T; s = 0, 1, \ldots, N_s. \end{cases} \quad (30)$$
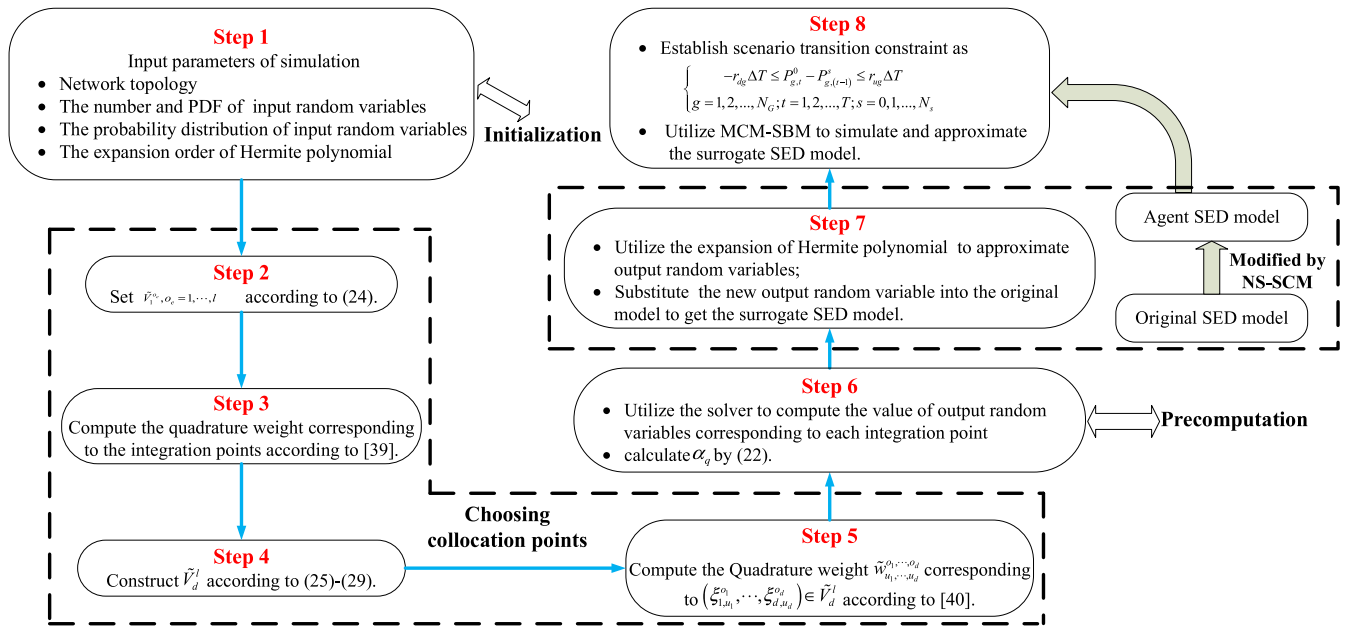
FIGURE 2. Algorithm flow of NS-SCM for solving the SED model with RES.

VI. NUMERICAL RESULTS

According to the theory of the NS-SCM, as soon as the original SED models have a feasible solution, we can utilize the NS-SCM to handle the heavy calculational burden. The present study then conducted simulations on a modified IEEE 39-bus system and a practical 1009-bus power system to verify the proposed approach. The forecast error of the outputs of the RES were assumed to obey the Gaussian distribution $N(\mu, \sigma^2)$, where μ is the forecasted outputs of the RES. The number of scheduling time intervals was defined as 24 (i.e., $T = 24$ h, $\Delta T = 60$ min) in the day-ahead SED model.

A. IEEE 39-BUS SYSTEM

Figure 3 presents two wind farms that have the capacities of 360 MW and 280 MW, respectively, that were joined to
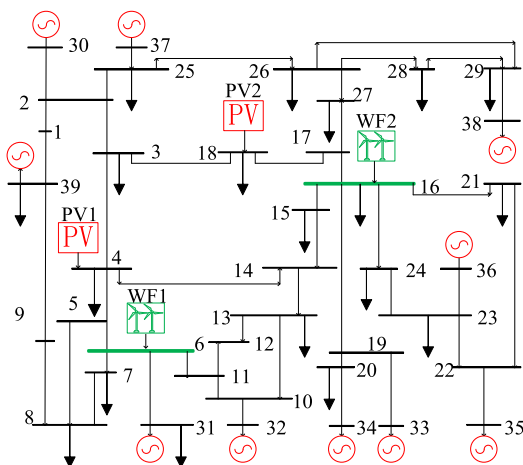
Bus 6 and Bus 16, respectively. Two PV power generations with capacities of 120 MW and 100 MW, respectively, were joined to Bus 4 and Bus 18, respectively. The penetration of the RES was performed at 13.98% of the load. The system exhibited peak and valley loads of 6,150 MW and 4,611 MW, respectively. Figure 4 shows the predicted total daily loads and the outputs of the RES. The other system parameters defined those generally observed in a standard IEEE 39-bus system [41]. For the modified IEEE-39 bus system, σ was set to 0.2 and N_{usp} was set to 999.
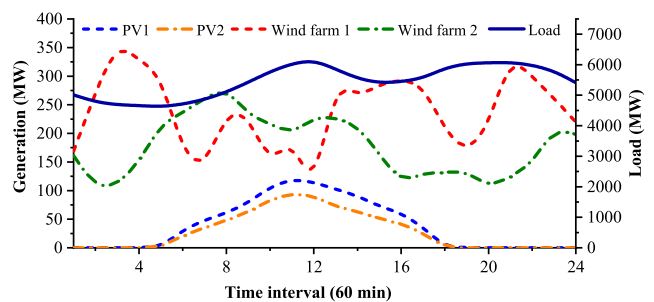

FIGURE 4. Forecast of the daily loads and outputs of the RES in the IEEE 39-bus system.

The relative errors of the three SCM algorithms were calculated to verify the accuracy of the method, specifically the relative solution errors (Sol.) and the relative errors of the objective value (Obj.). The relative solution error is defined as the maximum relative deviation of the results following the application of the three SCM algorithms as compared with those calculated using the MCM-SBM. The relative objective value error is defined as the relative error of the optimal

FIGURE 3. Modified IEEE-39 bus system with the RES.

objective values:

$$\text{Sol.error} = \left\| \frac{x_{\text{SCM}} - x_{\text{MCM-SBM}}}{x_{\text{MCM-SBM}}} \right\|_{\infty} \times 100\%$$

$$\text{Obj.error} = \left| \frac{f_{\text{SCM}} - f_{\text{MCM-SBM}}}{f_{\text{MCM-SBM}}} \right| \times 100\% \qquad (31)$$

where x_{SCM} and $x_{\text{MCM-SBM}}$ are the vectors of the three SCM algorithms and MCM-SBM results, respectively; f_{SCM} and $f_{\text{MCM-SBM}}$ are the optimal objective values of the three SCM algorithms and the MCM-SBM, respectively. Figure 5 illustrates the Sol. and the Obj. obtained by NS-SCM with different integral precisions l of MNI.
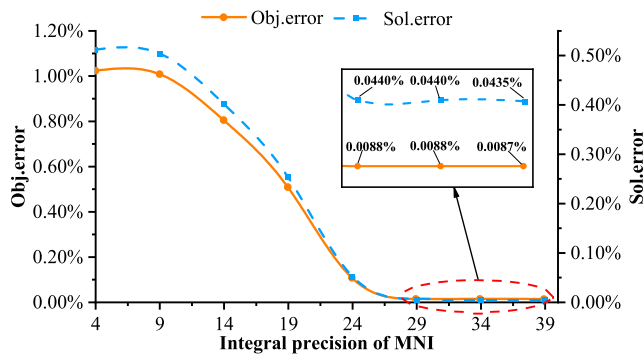
FIGURE 5. Results obtained by NS-SCM with different integral precision of MNI.

Figure 5 presents the relative solution errors and the decreased relative objective value errors following an increase in the integral precision. When the integral precision l increased to 29, the Sol. and the Obj. dropped to 0.0088% and 0.0440%, respectively, both of which were sufficiently small and could be defined as negligible. Upon further increasing the integral precision, we found that both changed very little. Therefore, we confirmed that the integral precision threshold was 29 for the IEEE-39 bus modified system. That is, the best integral precision was equal to 29. The MCM-SBM, F-SCM, S-SCM, and the proposed NS-SCM were respectively compared and evaluated based on their ability to resolve the SED model of the IEEE-39 bus system, the results of which are presented in Table 1.

TABLE 1. Comparison of the approaches in the IEEE 39-bus system.

Algorithm		MCM-SBM	F-SCM	S-SCM	NS-SCM
Cost (RMB¥ 1000)		6,621,650	6,622,213	6,622,705	6,622,233
Error	Obj.	0	0.0085%	0.0159%	0.0088%
	Sol.	0	0.0250%	0.0653%	0.0440%
N_{cp}		/	810,000	248,161	386,954
CPU time (min)		125.42	35.65	15.64	10.65

Each of the three SCM algorithms in Table 1 presented considerably close costs to the cost obtained by the MCM-SBM. In addition, the Sol. and the Obj. of the three SCM algorithms did not exceed 0.0159% and 0.0653%, respectively.
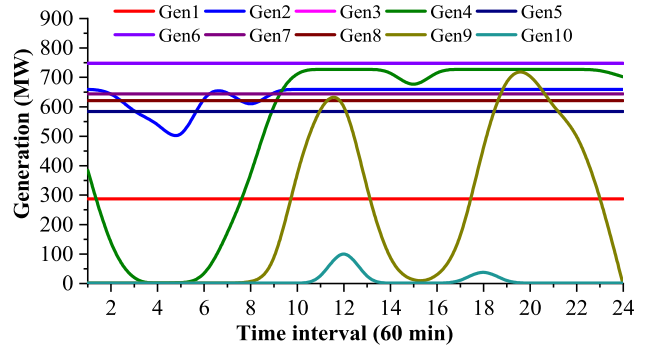
FIGURE 6. Dispatching plan of conventional generator units in an entire day.

As the SED models modified using SCM were considerably simpler than the original one, the three SCM algorithms had greatly improved computational efficiency compared with MCM-SBM (>71.57%). We then analyzed the relationship of the performance of the three SCM algorithms and the number of their collocation points. The F-SCM exhibited the least error but required the highest amount of collocation points, thus requiring an application and computation time of 35.65 min. The S-SCM exhibited a reduced CPU time due to the decrease in the number of collocation points and a certain loss in accuracy. In comparison, although the proposed NS-SCM used more collocation points than S-SCM, it took less time and had higher calculation precision. Figure 6 presents the outputs of each conventional generator unit, which were calculated by the NS-SCM over one full entire day.

B. PRACTICAL 1009-BUS POWER SYSTEM

The present study proceeded with calculations following a real 1009-bus system in China to further demonstrate the benefits of the proposed method in practical applications. The bus system consisted of 1724 branches, two wind farms with capacities of 1105 and 2219 MW, respectively, and two PV power generations with capacities of 1500 and 1100 MW, respectively. The penetration of the RES was performed at 10.82% of the load. The practical system had peak and valley loads of 54750 and 44611 MW, respectively. Figure 7 presents the forecasted total daily load and outputs of the RES
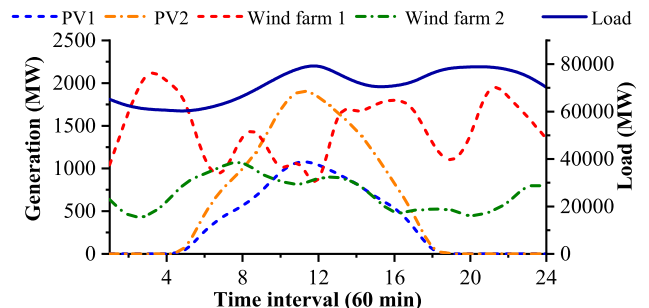
FIGURE 7. Forecasted daily loads and outputs of the RES in the practical 1009-bus system.

in the practical 1009-bus system. The other parameters of the simulation are given in Table 2.

TABLE 2. Parameters of simulation.

σ	0.12
l	49
N_{ucp}	50
N_{uss}	999

Figure 8 demonstrates the computational performances of both MCM-SBM and NS-SCM. As can be seen, NS-SCM was considerably faster than the MCM-SBM in solving SED problems. Furthermore, the CPU time of the MCM-SBM scaled linearly with an increase in the number of scenarios. This comparison showed that the proposed NS-SCM was very suitable for SED problems and showed an overwhelming advantage in the computational efficiency.
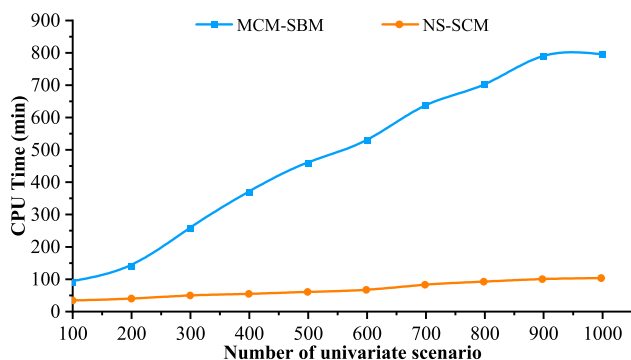

FIGURE 8. Comparison of computational time between MCM-SBM and NS-SCM.

TABLE 3. Comparison of the approaches in the 1009-bus system.

Algorithm		MCM-SBM	F-SCM	S-SCM	NS-SCM
Cost (RMB¥ 1000)		180.485620	180.593911	180.756348	180.619179
Error	Obj.	0	0.060%	0.150%	0.074%
	Sol.	0	0.085%	0.263%	0.135%
N_{cp}		/	6250000	1304493	2256985
CPU time (min)		795.43	256.36	136.56	99.65

Table 3 lists the comparisons of the results obtained by MCM-SBM, F-SCM, S-SCM, and the proposed NS-SCM. As shown in Table 5, all three of the SCM algorithms obtained the very small Sol. and Obj., not exceeding 0.150% and 0.263%, respectively. Following the sampling scenarios of the MCM-SBM, the F-SCM exhibited the least error due to the application of a significant amount of collocation points, though this approach generated a calculation time of 256.36 min. The SED models were considerably simpler and presented a calculation efficiency that could be further improved as compared to the sparse grid-based approach, which was initially applied to reduce the number of collocation points. As compared to the S-SCM, the NS-SCM used

TABLE 4. Parameters of conventional generators.

Bus	P_{gmax} (MW)	P_{gmin} (MW)	$r_{ug}(r_{dg})$ (MW/h)	a_g (RMB¥ 10^3/MW)
30	287.50	0	107.81	125.23
31	658.72	0	247.02	132.60
32	747.50	0	280.31	124.55
33	726.80	0	272.55	133.86
34	584.20	0	219.08	128.05
35	747.50	0	280.31	124.18
36	644.00	0	241.50	124.74
37	621.00	0	232.88	127.63
38	954.50	0	357.94	138.30
39	1150.00	0	431.25	141.75

TABLE 5. Forecast daily loads and outputs of the RES corresponding to Figure 4.

Time interval	PV 1 (MW)	PV 2 (MW)	Wind farm 1 (MW)	Wind farm 2 (MW)	Load (MW)
1	0	0	168.31	160.53	5002.5
2	0	0	271.17	104.53	4773.06
3	0	0	360	108.27	4677.52
4	0	0	327.27	149.33	4656.99
5	0	0	303.9	216.53	4611.59
6	30	21.25	163.64	235.2	4697.26
7	48	34	135.58	261.33	4853.2
8	60	47.5	238.44	280	5092.45
9	78	61.75	233.77	231.47	5416.97
10	105.6	83.6	140.26	216.53	5763.99
11	120	95	196.36	197.87	6029.29
12	114	90.25	88.83	227.73	6150.1
13	102	71.4	294.55	227.73	5850.06
14	90	63	261.82	212.8	5547.64
15	72	50.4	285.19	164.27	5391.31
16	60	42	294.55	112	5435.92
17	36	25.2	285.19	130.67	5549.22
18	0	0	205.71	130.67	5882.04
19	0	0	163.64	134.4	6037.58
20	0	0	210.39	104.53	6059.3
21	0	0	336.62	123.2	6071.93
22	0	0	299.22	145.6	5987.84
23	0	0	261.82	209.07	5796.37
24	0	0	219.74	197.87	5409.86

more collocation points to streamline the SED model but generated more precise results and a higher computational efficiency. In particular, the CPU time of NS-SCM was only 12.53% of that of MCM-SBM. These comparisons verified that NS-SCM was applicable to solve SED problems in practical large-scale systems.

VII. CONCLUSION
Fully considering the uncertainty of RES, in this paper, we proposed the NS-SCM to simplify the scenario-based SED model, which improved the computational efficiency with minimal loss of accuracy. According to the SCM, the optimal gPC was applied to approximate random variables through a finite-order expansion, thus eliminating the need to apply a complicated optimization model with random variables. We proposed a strategic method for construction of collocation points based on the nested sparse grid method to

enhance the computational efficiency, by which the chosen collocation points satisfied the nested property. This proposed method was successfully applied and was able to successfully resolve the optimization problem (*i.e.*, the SED problem). By performing case studies on IEEE 39-bus and practical 1009-bus systems, we verified the accuracy, practicality, and effectiveness of the proposed method. The numerical findings indicate that the method we propose is suitable for systems with different scales and presents promising engineering application prospects, specifically for the economic dispatching of power systems.

APPENDIX

In this section, the technical details of the considered power system in Figures 3 and 4 are given.

The other system parameters, including the data of 39 buses and 46 branches, are generally observed in a standard IEEE 39-bus system [41].

REFERENCES

[1] B. Kroposki, B. Johnson, Y. Zhang, V. Gevorgian, P. Denholm, B.-M. Hodge, and B. Hannegan, "Achieving a 100% renewable grid: Operating electric power systems with extremely high levels of variable renewable energy," *IEEE Power Energy Mag.*, vol. 15, no. 2, pp. 61–73, Mar./Apr. 2017.

[2] *100% Renewables Study-Modelling Outcomes*, AEMO, Canberra, ACT, Australia, Jul. 2013.

[3] N. Li and K. W. Hedman, "Economic assessment of energy storage in systems with high levels of renewable resources," *IEEE Trans. Sustain. Energy*, vol. 6, no. 3, pp. 1103–1111, Jul. 2015.

[4] H. T. Nguyen, D. T. Nguyen, and L. B. Le, "Energy management for households with solar assisted thermal load considering renewable energy and price uncertainty," *IEEE Trans. Smart Grid*, vol. 6, no. 1, pp. 301–316, Jan. 2015.

[5] Q. Wang, Y. Guan, and J. Wang, "A chance-constrained two-stage stochastic program for unit commitment with uncertain wind power output," *IEEE Trans. Power Syst.*, vol. 27, no. 1, pp. 206–215, Feb. 2012.

[6] A. Kargarian, Y. Fu, and H. Wu, "Chance-constrained system of systems based operation of power systems," *IEEE Trans. Power Syst.*, vol. 31, no. 5, pp. 3404–3413, Sep. 2016.

[7] Y. Cao, Y. Tan, C. Li, and C. Rehtanz, "Chance-constrained optimization-based unbalanced optimal power flow for radial distribution networks," *IEEE Trans. Power Del.*, vol. 28, no. 3, pp. 1855–1864, Jul. 2013.

[8] Y. Z. Li and Q. H. Wu, "Downside risk constrained probabilistic optimal power flow with wind power integrated," *IEEE Trans. Power Syst.*, vol. 31, no. 2, pp. 1649–1650, Mar. 2016.

[9] D. Ke, C. Y. Chung, and Y. Sun, "A novel probabilistic optimal power flow model with uncertain wind power generation described by customized Gaussian mixture model," *IEEE Trans. Sustain. Energy*, vol. 7, no. 1, pp. 200–212, Jan. 2016.

[10] S. Xia, X. Luo, K. W. Chan, M. Zhou, and G. Li, "Probabilistic transient stability constrained optimal power flow for power systems with multiple correlated uncertain wind generations," *IEEE Trans. Sustain. Energy*, vol. 7, no. 3, pp. 1133–1144, Jul. 2016.

[11] Y. Wang, N. Zhang, Q. Chen, J. Yang, C. Kang, and J. Huang, "Dependent discrete convolution based probabilistic load flow for the active distribution system," *IEEE Trans. Sustain. Energy*, vol. 8, no. 3, pp. 1000–1009, Jul. 2017.

[12] Z. Q. Xie, T. Y. Ji, M. S. Li, and Q. H. Wu, "Quasi-Monte Carlo based probabilistic optimal power flow considering the correlation of wind speeds using copula function," *IEEE Trans. Power Syst.*, vol. 33, no. 2, pp. 2239–2247, Mar. 2018.

[13] P. A. Ruiz, C. R. Philbrick, and P. W. Sauer, "Modeling approaches for computational cost reduction in stochastic unit commitment formulations," *IEEE Trans. Power Syst.*, vol. 25, no. 1, pp. 588–589, Feb. 2010.

[14] X. Bai and W. Qiao, "Robust optimization for bidirectional dispatch coordination of large-scale V2G," *IEEE Trans. Smart Grid*, vol. 6, no. 4, pp. 1944–1954, Jul. 2015.

[15] H. Nosair and F. Bouffard, "Economic dispatch under uncertainty: The probabilistic envelopes approach," *IEEE Trans. Power Syst.*, vol. 32, no. 3, pp. 1701–1710, May 2017.

[16] Y. Xu, M. Yin, Z. Y. Dong, R. Zhang, D. J. Hill, and Y. Zhang, "Robust dispatch of high wind power-penetrated power systems against transient instability," *IEEE Trans. Power Syst.*, vol. 33, no. 1, pp. 174–186, Jan. 2018.

[17] M. Hedayati-Mehdiabadi, K. W. Hedman, and J. Zhang, "Reserve policy optimization for scheduling wind energy and reserve," *IEEE Trans. Power Syst.*, vol. 33, no. 1, pp. 19–31, Jan. 2018.

[18] A. Gupta and C. L. Anderson, "Statistical bus ranking for flexible robust unit commitment," *IEEE Trans. Power Syst.*, vol. 34, no. 1, pp. 236–245, Jan. 2019.

[19] Y. Sasaki, N. Yorino, Y. Zoka, and F. I. Wahyudi, "Robust stochastic dynamic load dispatch against uncertainties," *IEEE Trans. Smart Grid*, vol. 9, no. 6, pp. 5535–5542, Nov. 2018.

[20] F. Bouffard and F. D. Galiana, "Stochastic security for operations planning with significant wind power generation," *IEEE Trans. Power Syst.*, vol. 23, no. 2, pp. 306–316, May 2008.

[21] J. Morales, A. J. Conejo, and J. Perez-Ruiz, "Economic valuation of reserves in power systems with high penetration of wind power," *IEEE Trans. Power Syst.*, vol. 24, no. 2, pp. 900–910, May 2009.

[22] A. Papavasiliou, S. Oren, and R. O'Neill, "Reserve requirements for wind Power integration: A scenario-based stochastic programming framework," *IEEE Trans. Power Syst.*, vol. 26, no. 4, pp. 2197–2206, Nov. 2011.

[23] D. Zhu and G. Hug, "Decomposed stochastic model predictive control for optimal dispatch of storage and generation," *IEEE Trans. Smart Grid*, vol. 5, no. 4, pp. 2044–2053, Jul. 2014.

[24] H. Ming, L. Xie, M. Campi, S. Garatti, and P. Kumar, "Scenario-based economic dispatch with uncertain demand response," *IEEE Trans. Smart Grid*, vol. 10, no. 2, pp. 1858–1868, Mar. 2019. doi: 10.1109/TSG.2017.2778688.

[25] C. Tang, J. Xu, Y. Tan, Y. Sun, and B. Zhang, "Lagrangian relaxation with incremental proximal method for economic dispatch with large numbers of wind power scenarios," *IEEE Trans. Power Syst.*, vol. 34, no. 4, pp. 2685–2695, Jul. 2019. doi: 10.1109/TPWRS.2019.2891227.

[26] J. Tang, F. Ni, F. Ponci, and A. Monti, "Dimension-adaptive sparse grid interpolation for uncertainty quantification in modern power systems: Probabilistic power flow," *IEEE Trans. Power Syst.*, vol. 31, no. 2, pp. 907–919, Mar. 2016.

[27] W. Li, J. Zhou, K. Xie, and X. Xiong, "Power system risk assessment using a hybrid method of fuzzy set and Monte Carlo simulation," *IEEE Trans. Power Syst.*, vol. 23, no. 2, pp. 336–343, May 2008.

[28] D. Xiu, *Numerical Methods for Stochastic Computations*. Princeton, NJ, USA: Princeton Univ. Press, 2010, pp. 1–28.

[29] A. Biondi, D. Vande Ginste, D. De Zutter, P. Manfredi, and F. G. Canavero, "Variability analysis of interconnects terminated by general nonlinear loads," *IEEE Trans. Compon., Packag., Manuf. Technol.*, vol. 3, no. 7, pp. 1244–1251, Jul. 2013.

[30] J. Bai, G. Zhang, A. P. Duffy, and L. Wang, "Dimension-reduced sparse grid strategy for a stochastic collocation method in EMC software," *IEEE Trans. Electromagn. Compat.*, vol. 60, no. 1, pp. 218–224, Feb. 2018.

[31] A.-K. Ali, A. J. Conejo, and R. Cherkaoui, "Multi-area unit scheduling and reserve allocation under wind power uncertainty," *IEEE Trans. Power Syst.*, vol. 29, no. 4, pp. 1701–1710, Jul. 2014.

[32] A. Kargarian, Y. Fu, and Z. Li, "Distributed security-constrained unit commitment for large-scale power systems," *IEEE Trans. Power Syst.*, vol. 30, no. 4, pp. 1136–1925, Jul. 2015.

[33] Z. Li, W. Wu, B. Zhang, and B. Wang, "Decentralized multi-area dynamic economic dispatch using modified generalized benders decomposition," *IEEE Trans. Power Syst.*, vol. 31, no. 1, pp. 526–538, Jan. 2016.

[34] Z. Li, W. Wu, M. Shahidehpour, and B. Zhang, "Adaptive robust tie-line scheduling considering wind power uncertainty for interconnected power systems," *IEEE Trans. Power Syst.*, vol. 31, no. 4, pp. 2701–2713, Jul. 2016.

[35] X. Lai, L. Xie, Q. Xia, H. Zhong, and C. Kang, "Decentralized multi-area economic dispatch via dynamic multiplier-based Lagrangian relaxation," *IEEE Trans. Power Syst.*, vol. 30, no. 6, pp. 3225–3233, Nov. 2015.

[36] H. Zhong, Q. Xia, Y. Wang, and C. Kang, "Dynamic economic dispatch considering transmission losses using quadratically constrained quadratic program method," *IEEE Trans. Power Syst.*, vol. 28, no. 3, pp. 2232–2241, Aug. 2013.

[37] T. N. dos Santos and A. L. Diniz, "A dynamic piecewise linear model for DC transmission losses in optimal scheduling problems," *IEEE Trans. Power Syst.*, vol. 26, no. 2, pp. 508–519, May 2011.

[38] W. Yi, Z. Xuan, and T. Jun, ''Stochastic collocation method for statistical static timing analysis with input truncation technique,'' *J. Comput.-Aided Des. Comput. Graph.*, vol. 20, no. 12, pp. 1527–1534, 2008.

[39] E. W. Weisstein, *The CRC Concise Encyclopedia of Mathematics*, 1st ed. Boca Raton, FL, USA: CRC Press, 1999.

[40] T. Gerstner and M. Griebel, ''Numerical integration using sparse grids,'' *Numer. Algorithms*, vol. 18, pp. 209–232, Mar. 1998.

[41] A. Pai, *Energy Function Analysis for Power System Stability*. Norwell, MA, USA: Kluwer, 1989.

ZHILIN LU received the B.S. degree in electrical engineering from the South China University of Technology, Guangzhou, China, in 2018, where he is currently pursuing the M.S. degree with the School of Electric Power Engineering. His research interests include energy management and operation control of power systems.

MINGBO LIU (M'12) received the B.S. degree from the Huazhong University of Science and Technology, in 1985, the M.S. degree from the Harbin Institute of Technology, in 1988, and the Ph.D. degree from Tsinghua University, in 1992. He is currently a Professor with the South China University of Technology. He has authored and coauthored four monographs, two standards, and more than 240 papers. His research interests include energy management and operation control of power systems.

WENTIAN LU received the B.S. degree from the Jiangxi University of Science and Technology, in 2013, and the Ph.D. degree from the South China University of Technology (SCUT), in 2018, where she is currently a Postdoctoral Researcher. Her research interests include energy management and operation control of power systems.

ZHUOMING DENG received the B.S. and Ph.D. degrees in electrical engineering from the South China University of Technology, Guangzhou, China, in 2014 and 2019, respectively. He is currently with the Electric Power Research Institute, China Southern Power Grid, Guangzhou. His research interests include voltage stability analysis, planning, and control of power systems.

• • •